GaAs Microisland Anodes Protected by Amorphous TiO_2 Films Mitigate Corrosion Spreading During Water Oxidation in Alkaline Electrolytes

Pakpoom Buabthong[1], Jake M. Evans[2], Katherine Z. Rinaldi[2], Kathleen M. Kennedy[1], Harold J. Fu[2], Zachary P. Ifkovits[2], Tai-Jung Kuo[1], Bruce S. Brunschwig[3], and Nathan S. Lewis[2,3 *]

[1]Division of Engineering and Applied Sciences, California Institute of Technology, Pasadena, CA 91125

[2]Division of Chemistry and Chemical Engineering, California Institute of Technology, Pasadena, California 91125, USA.

[3]Beckman Institute and Molecular Materials Research Center, California Institute of Technology, Pasadena, California 91125, USA.

[*]Corresponding author: nslewis@caltech.edu

Keywords: pinholes, physical defects, amorphous, titanium dioxide, atomic-layer deposition, gallium arsenide, micro-islands

Experimental Methods

Materials and Chemicals

Water with a resistivity ρ > 18 MΩ·cm was obtained from a Barnstead Millipore purification system. All chemicals were used as received, including potassium hydroxide (TraceSELECT, ≥30% in water, Honeywell Fluka), buffered oxide etchant (BOE, 6:1 NH_4F to HF, Transene Company, Inc.), gallium-indium eutectic (Alfa Aesar, 99.99%), Nickel etchant (Ni Etch TFG, Transene Company, Inc.), GaAs etchant (GA Etch 300, Transene Company, Inc.), polydimethylsiloxane (PDMS) (Sylguard), PDMS curing agent (Sylguard 184), toluene (Millipore Sigma, GR ACS), and Ag epoxy adhesive (MG Chemicals, 8331). Crystalline single-side polished (100)-oriented, 350±25-μm-thick p^+-GaAs substrates were degenerately doped with zinc to a majority-carrier density of 0.5-5×10^{19} cm^{-3} (AXT Inc.). (100) oriented, 500-μm-thick p^+-Si wafers were degenerately doped with boron, and had a resistivity of 0.001-0.005 Ω cm (Addison Engineering).

Preparation of Substrates

The GaAs wafers were cleaned with 10% (1.16 M) HCl(aq) for 30 min to remove native oxide on the surface.[1] The Si wafers were submerged in BOE for 1 min to remove native oxide. The samples were then rinsed with copious amounts of deionized H_2O and dried using a stream of N_2(g).

Atomic Layer Deposition (ALD) of TiO_2 Thin Films

a-TiO_2 films were grown using tetrakis(dimethylamido)-titanium (TDMAT). For *a*-TiO_2 films prepared from the TDMAT precursor, a Cambridge Nanotech S200 or Oxford Instruments FlexAL ALD system was used for deposition outside and inside the cleanroom. Each ALD cycle consisted of a 0.10 s exposure to TDMAT (Sigma-Aldrich, 99.999%), a N_2(g) (Airgas, 99.999%) purge, a 0.015 s exposure to H_2O, and a final N_2(g) purge. Research-grade 20 sccm N_2(g) was used for the N_2(g) purges, and each N_2(g) purge was 15 s in duration. During the deposition, the substrate and the TDMAT precursor were heated to 150 °C and 75 °C, respectively, while the H_2O remained at room temperature. Most samples were prepared with 2000 ALD cycles to produce films that were nominally 110 nm thick. The film thickness and refractive index were measured via spectroscopic ellipsometry (J.A. Woollam Co., alpha-SE) and were fit to a Cauchy model.

Radio-Frequency Sputtering Deposition

A radio-frequency sputtering system (AJA International Inc.) was used to deposit Ni and Cu for back ohmic contacts to p^+-GaAs. The base pressure was $<1\times10^{-7}$ Torr, and the deposition pressure was 5 mTorr. A radio-frequency (rf) power of 100 W was maintained during the deposition.

Electrode Fabrication

Electrodes were fabricated by using a scribe to cleave the samples into pieces of ~0.1 cm^2 in geometric area. Ohmic contact was made by sequentially depositing Ni/Cu films onto the unpolished back sides of the p^+-GaAs samples.[2] The back contact to the sample was affixed to a Cu wire with Ag paste. The Cu wire was threaded through a glass tube (Corning Incorporation, Pyrex tubing, 7740 glass), and all but the front of the sample was encapsulated with either Loctite epoxy (Hysol 9462) or Gorilla Glue (Gorilla Glue, Co). After curing, the electrode was scanned with an Epson scanner (V19) and analyzed with ImageJ to determine the area of the exposed region.[3]

Scanning electron microscopy

Scanning electron micrographs (SEMs) were obtained with an FEI Nova NanoSEM 450 at an accelerating voltage of 5.00 kV with a working distance of 5 mm and an in-lens secondary electron detector.

TiO_2 dissolution

To measure the dissolution of ALD TiO_2, a film of nominally ~80-nm-thick (1500 cycles) of TiO_2 was deposited onto p^+-Si. In-Ga was applied as the back contact and Ag paste was applied to affix the sample onto a Cu wire. To minimize residual TiO_2 contamination from the Hysol epoxy, Gorilla Glue instead of Hysol 9462 epoxy was used to seal to the sample from the electrolyte.

The electrodes were evaluated in 30 mL of 1.0 M KOH(aq) and were either maintained at the open-circuit potential (E_{oc}) or at E = 1.63 V vs RHE. 1 mL aliquots were taken at each interval. No electrolyte was replenished during the experiment. ICP-MS was used to analyze the Ti dissolution products in the aliquots.

Inductively Coupled Plasma Mass Spectroscopy

Inductively coupled plasma mass spectrometry (ICP-MS) data were collected using an Agilent 8800 Triple Quadrupole ICP-MS system. ICP-MS samples were collected periodically throughout electrochemical corrosion experiments. Samples were diluted 50x with 2% (0.32 M) nitric acid before analysis. ICP-MS concentration standards were made with serial dilutions of a known concentration standard (Sigma-Aldrich) with 2% nitric acid. Each concentration standard had KOH added in a 50:1 volumetric ratio of nitric acid: KOH (2%, 1.0 M, respectively) to match the solution matrix of the ICP-MS samples. Quantification was verified by independently making four additional samples of known concentrations and analyzing the samples at the beginning, middle, and end of all ICP-MS analysis. ICP-MS results were only used when the samples of known concentration were measured to be consistent throughout the ICP-MS run. The samples of known concentration were also made on a mass basis and were matrix-matched with the same 50 nitric acid:1 KOH volumetric ratio as both the unknown samples and the concentration standards. The total amount of dissolved Ti from the electrodes was then calculated and normalized to the geometric electrode area.

X-ray photoelectron spectroscopy

X-ray photoelectron spectroscopy (XPS) was performed using a Kratos Axis Ultra system with a base pressure of 1×10^{-9} torr in the analysis chamber. A monochromatic Al Kα source was used to irradiate the sample with X-rays (1486.7eV) at 150 W. A hemispherical analyzer oriented for detection along the sample surface normal was used for maximum depth sensitivity. The data were analyzed using CasaXPS computer software.

XPS data were obtained ex-situ i.e., after a short sample transfer through air, which could potentially confound linking the surface composition and oxidation states found in ultra-high vacuum to the surface conditions present during electrochemistry.

Electrochemical Characterization

Electrochemical data were obtained using a BioLogic SP-200 potentiostat in a three-electrode configuration with 1.0 M KOH(aq) as the electrolyte. A Hg/HgO electrode (CH Instruments, Inc., CHI-152) was used as the reference electrode for the alkaline solution. A carbon

rod (Strem Chemicals, 99.999%) inside a porous fritted gas dispersion tube (Sigma Aldrich, Z408727) was used as the counter electrode. *J-E* data were collected between -0.6 V and 0.8 V vs. Hg/HgO at a 20-mV s^{-1} scan rate. Chronoamperometry (CA) data were collected every 1 s while holding the electrode potential at 0.212 V vs. Hg/HgO, unless noted otherwise.

Raman Spectroscopy Methods

Raman spectra were collected with a Renishaw inVia Raman microprobe (Renishaw, Wotton-under-Edge, United Kingdom) equipped with a Leica DM 2500 M microscope (Leica Microsystems, Wetzlar, Germany), a Leica N Plan 50x objective (numerical aperture = 0.75), a 1800 lines mm^{-1} grating, and a 2D CCD detector configured in a 180° backscatter geometry. A 532 nm diode-pumped solid-state (DPSS) laser (Renishaw RL532C50) was used as the excitation source and a 2 mW radiant flux was incident on the surface of the sample. A line-focus lens was utilized to transform the circular incident beam in one dimension to generate an ~50 μm wide line at the sample. Spatially-resolved data were acquired by both rastering the sample underneath the line-shaped excitation and dispersing scatter collected along the line over one axis of the detector, perpendicular to the direction of frequency dispersion. Resolution in the direction perpendicular to the long axis was defined by the mechanical sample movement and in the direction parallel was defined by the pixel size of the detector. The sampling resolution was consequently 1.5 × 1.5 μm^2. Three 100 × 100 μm^2 Raman maps were obtained for each sample (2000x, 800x, 200x), to probe the uniformity across the sample.

Detailed Fabrication Procedures

General Considerations on the Overall Fabrication Processes

p^+-GaAs wafers were initially cleaned with 10% HCl (1.16 M) for 30 min and bonded onto p^+-Si substrates that had been cleaned with BOE for 1 min. The bonding process was performed in an environmentally controlled cleanroom, repeated from previously reported room-temperature direct wafer bonding.[4–6]. The GaAs/Si stacks were then mechanically thinned and polished to reduce the thickness of the p^+-GaAs to ~50 μm. The mask was subsequently deposited onto the stack, followed by the chemical etching process. The mechanical thinning and polishing step was detrimental to the p^+-GaAs surface and led to a substantial amount of micro-/nano-scale etch pits

(Fig. S8a). These etch pits eventually led to corrosion within the masked areas, thus resulting in ill-defined micro-island structures. Additionally, in some cases, the etch pits within the Ni masked areas may lead to metal-assisted chemical etching[7] in which the Ni masks catalyze the etching process under the mask area as opposed to the area outside the masked area (Fig. S8b). Hence, the micro-island etching was made to be the first process step, ensuring that the GaAs etchant only reacted with a pristine p^+-GaAs (100) surface, thus leading to sharp and well-defined micro-island structures (Fig. S3a).

Etching

A Ni mask was sputtered onto cleaned p^+-GaAs substrates for 30 min with a micro-island pattern stencil (an array of 200-μm-diameter circle and 350-μm pitch), yielding a mask thickness of ~30 nm. The samples were mounted onto a thin glass slide using nail polish. A bath containing a commercial GaAs etchant (Transene, GA Etch 300) was heated to 45 °C and stirred at 600 rpm. The masked samples were then submerged in the etchant for 30 min to obtain ~ 30-μm-tall micro-island structures.

Due of the lower precision over the control of the etchant transport in wet etch compared to dry etch, the chemical etching process might have higher tendency for undesirable isotropic etching and inconsistency in the etched structures (Fig. S9a,b). The optimal setup for the etching bath was obtained when the samples were placed off-center and slightly tilted to facilitate transport of the etchant (Fig. S9c,d)

Thinning

Before the thinning process, the Ni masks were removed from the surface by etching for 2 min in a commercial Ni etchant (Transene, Ni Etch TFG). Optical microscopy images of the samples coated with patterned Ni masks before and after the etch showed that the etchant entirely removed the masks while leaving the underlying p^+-GaAs substrate intact (Fig. S10a,b). X-ray photoelectron spectroscopy (XPS) of the Ni 2p region on the sample before and after the Ni etch also confirmd that the majority of the surface Ni was removed (Fig. S10c).

The samples were mounted onto a polishing stub using finely ground crystal bond (Fig. S11a). After the crystal bond had dried, the samples were thinned using 320-grit polishing paper until parts of the micro-island structures were exposed (Fig. S11b). The samples were then

carefully thinned down using 600-grit and 1000-grit polishing papers until all of the micro-island structures were exposed (Fig. S11c,d).

Assembling with p^+-Si Substrates

The polishing stub with the micro-island structures embedded in crystal bond was transferred to the sputterer for the deposition of a Ni/Cu back ohmic contact. In preparation for the p^+-Si substrates, the wafer was etched for 1 min in BOE, and In-Ga ohmic contact was applied to the front side of the p^+-Si substrates. Then, Ag epoxy was applied to the p^+-Si substrates, which were subsequently placed on top of the micro-island structures. The samples were cured on a hot plate at 70 °C for 30 min while a constant pressure of ~50 N m^{-2} was applied by placing an appropriate weight on top of the sample. The weight reduced small gaps and air pockets between the p^+-Si substrate and the micro-island structures. The samples were then removed from the polishing stub by heating the stub at 130 °C for 15 min on a hot plate, followed by sonicating in acetone to remove any residual crystal bond.

PDMS Coating

The PDMS coating process was modified from a previously reported recipe.[8] Briefly, the micro-island structures were infilled with PDMS, toluene, and Sylguard 184 silicone elastomer curing agent in a ratio of 10:50:1. After sonicating the mixture for 15 min, the samples were placed on a spin coater, cleaned by drop-casting toluene at 3000 rpm for 1 min, and then infilled by covering the micro-island structures with the PDMS mixture followed by spin coating at 3000 rpm. The samples were then cured on a glass slide on a hot plate at 150 °C for 1.5 h.

Image Processing

During the electrochemical experiments, optical micrographs of the surface were taken every 5 min. A hexagonal array pattern was then superimposed onto the first micrograph for a positional reference (Fig. S12). Each frame was compared to the subsequent one where the timestamp and the position of new failed micro-islands were recorded manually. The distribution of failed micro-islands was plotted onto a digital replication of the electrode surface using Matplotlib library (Fig. 3b). Two micro-islands samples were used for the experiment. The percentage of failed micro-islands in each sample was calculated, then the averages and the

standard deviations of the these percentages were plotted in Fig. 3a. The raw counts are presented in Table S1.

	Sample #1 (73.58 mm^2)		Sample #2 (12.39 mm^2)			
Time	Remaining	Remaining %	Remaining	Remaining %	Avg	Std
0	668	100.00	111	100.00	100.00	0.00
1	660	98.80	109	98.20	98.50	0.43
5	653	97.75	108	97.30	97.53	0.32
10	649	97.16	108	97.30	97.23	0.10
15	646	96.71	107	96.40	96.55	0.22
17	645	96.56	107	96.40	96.48	0.11
20	643	96.26	105	94.59	95.43	1.18
22	643	96.26	100	90.09	93.17	4.36
25	640	95.81	100	90.09	92.95	4.04
30	631	94.46	97	87.39	90.92	5.00
35	605	90.57	97	87.39	88.98	2.25
40	493	73.80	94	84.68	79.24	7.69
45	418	62.57	90	81.08	71.83	13.09
53	239	35.78	57	51.35	43.56	11.01
60	195	29.19	54	48.65	38.92	13.76
65	149	22.31	43	38.74	30.52	11.62
70	97	14.52	28	25.23	19.87	7.57

Table S1. Remain islands as a function of time on the micro-island samples.

Supporting figures

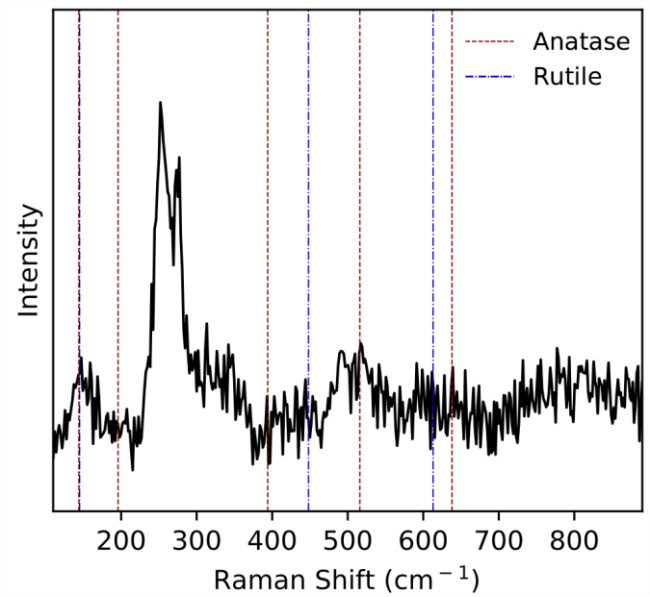

Figure S1. Representative Raman spectrum measured on p^+-GaAs samples coated with amorphous *a*-TiO_2-2000x (GaAs/*a*-TiO_2-2000x) with the dashed lines representing the respective peak positions for crystalline anatase and rutile TiO_2.

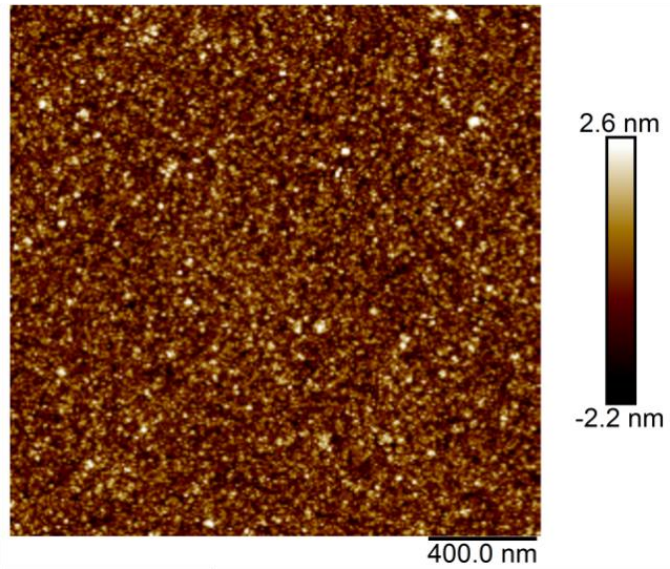

Figure S2. Atomic-force microscopy topography scanning measured on p^+-GaAs samples coated with amorphous *a*-TiO_2-2000x (GaAs/*a*-TiO_2-2000x).

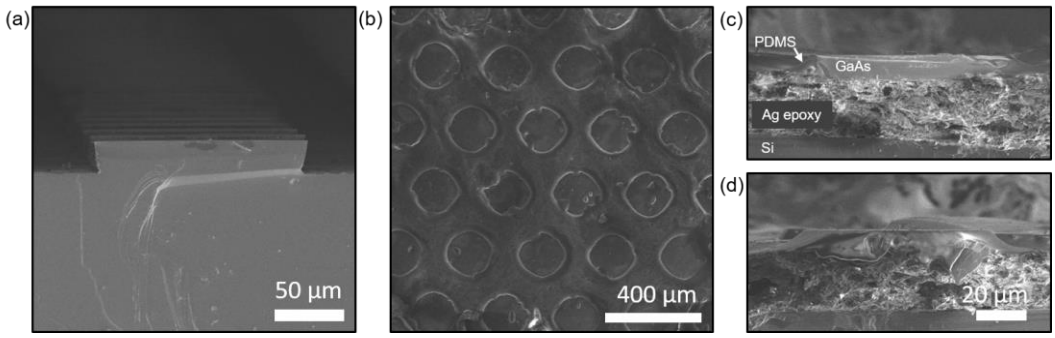

Figure S3. (a) Cross-sectional SEM of GaAs structure after etching (Fig. 1c) and SEM of (b) top surface (c, d) cross-sectional SEM of the final structure (Fig. 1i).

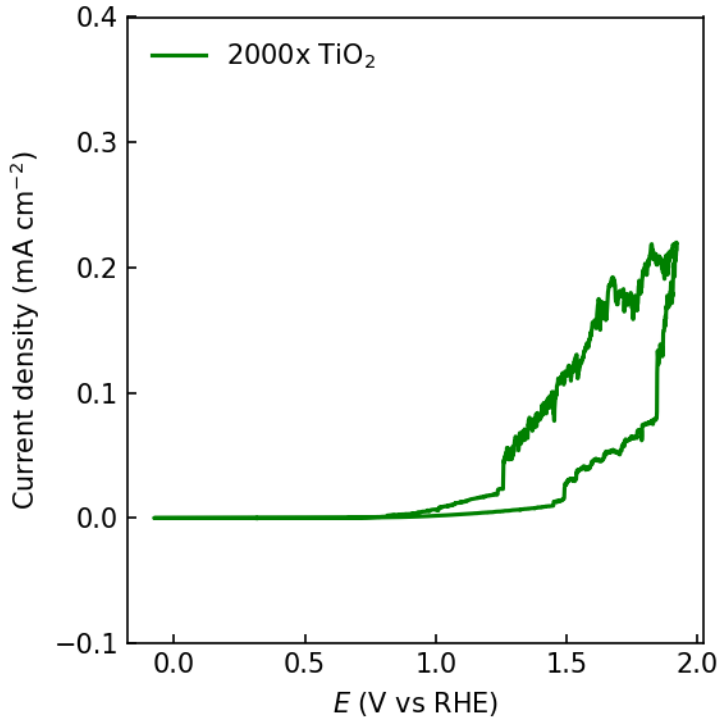

Figure S4. Current density vs potential (*J*-*E*) behavior of p^+-GaAs micro-island structures with amorphous *a*-TiO_2 (GaAs/*a*-TiO_2-2000x) with the y-axis scaled from -0.1 to 0.4 mA cm^{-2}. The scan rate was 40 mV s^{-1}.

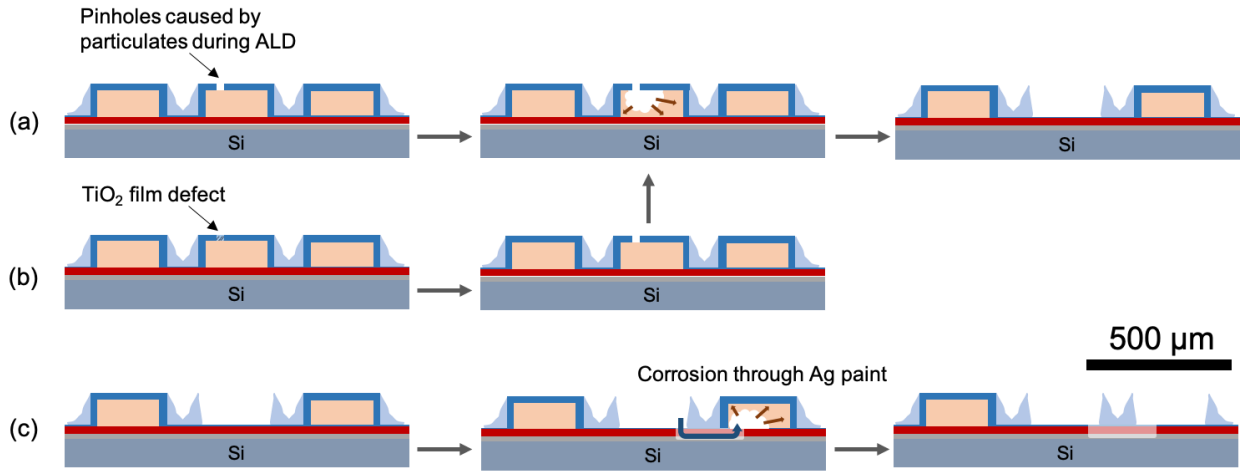

Figure S5. Schematics describing three corrosion pathways on the micro-island structures: (a) initial failure pinholes caused by particulates during ALD, (b) failed micro-islands from newly developed pinholes during the electrochemical operation, and (c) failed micro-islands due to corrosion from nearby micro-islands through semi-porous Ag layer.

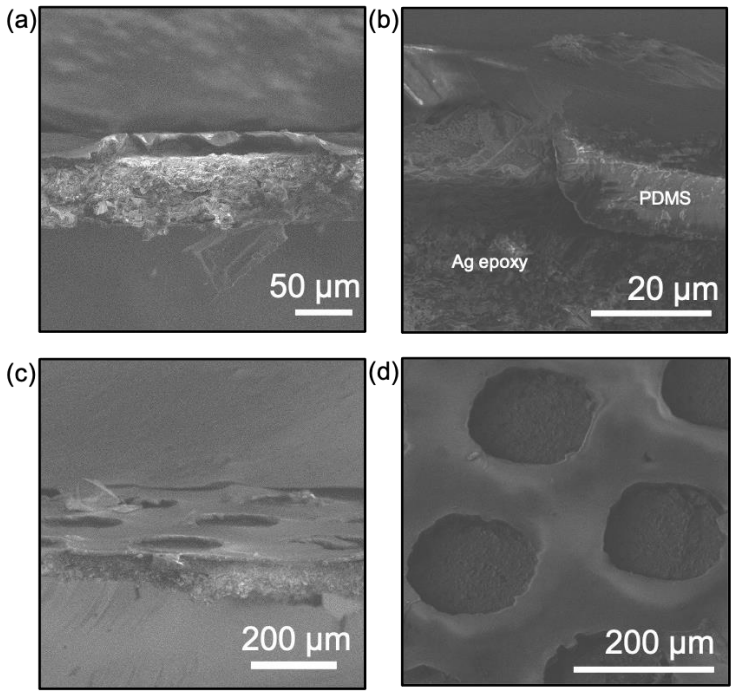

Figure S6. (a-c) Cross-sectioned SEM and (d) top-down SEM of the islands that failed after 40 h. (b) Remaining PDMS film at the edge of the failed GaAs micro-islands.

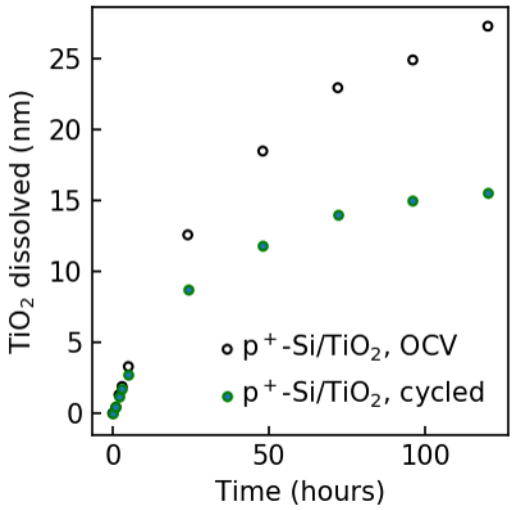

Figure S7. Dissolved Ti as a function of time for *a*-TiO_2-coated p^+-Si (p^+-Si/TiO_2-1500x) evaluated (black empty circles) at the open-circuit potential and (green filled circles) at 1.63 V vs RHE for 6 h followed by at the open-circuit potential for 18 h, alternatingly.

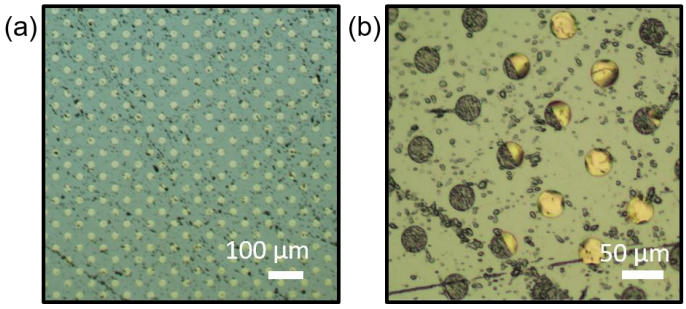

Figure S8. Optical micrographs of the electrode surfaces showing (a) etch pits resulting from the thinning step and (b) metal-assisted chemical etching underneath Ni masks.

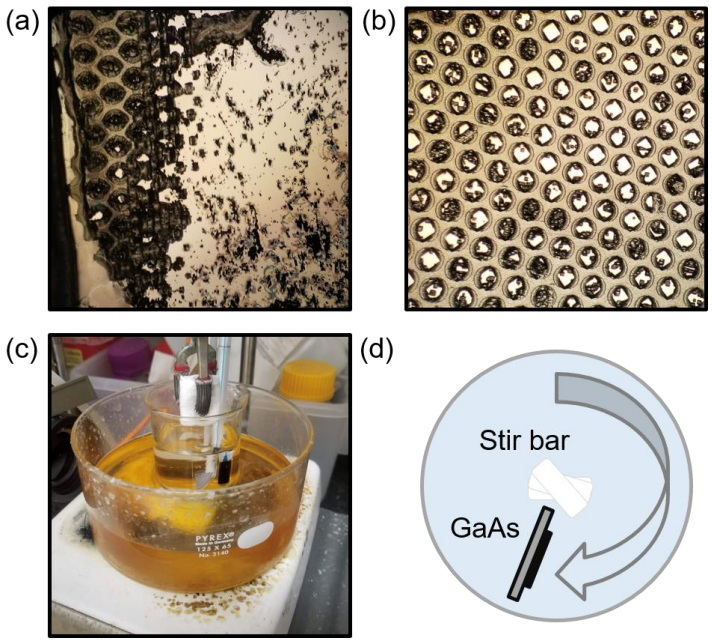

Figure S9. (a,b) Optical micrographs showing inconsistency of the etched surface, (c) etch bath setup, and (d) a top-view illustration of sample position in the etch bath.

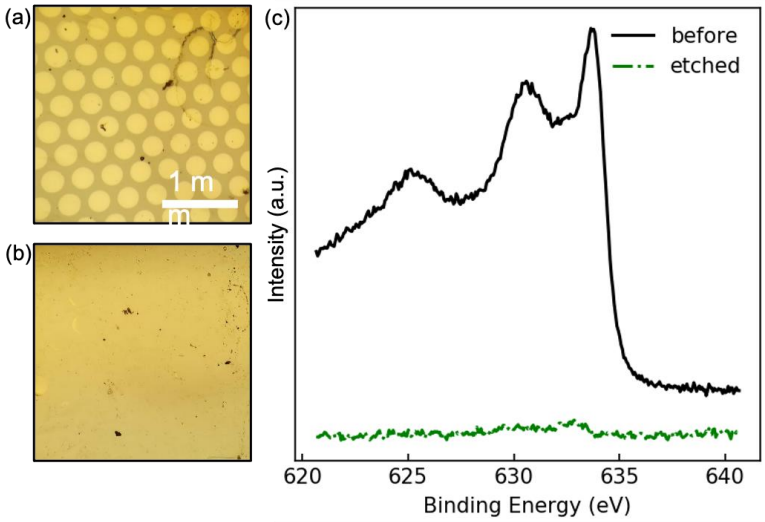

Figure S10. Optical microscope of a Ni mask on a GaAs substrate (a) before and (b) after mask etching. (c) XPS of Ni 2p on the respective surface.

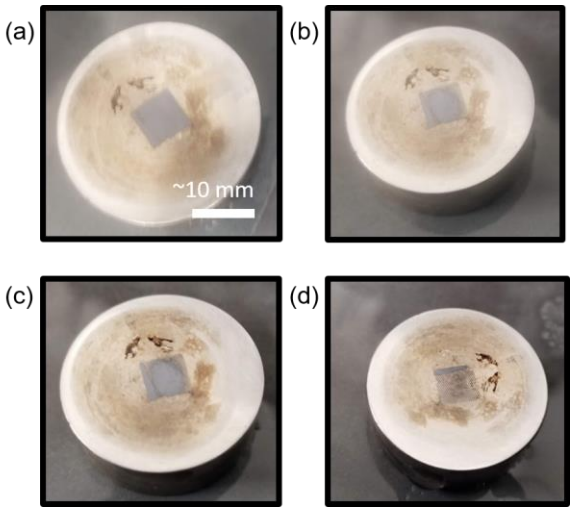

Figure S11. Micro-island structures embedded in crystal bond on a polishing stub with each image showing a subsequent thinning step (a-d).

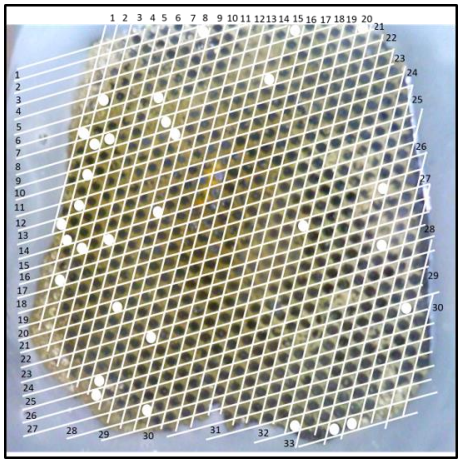

Figure S12. Optical micrograph of the electrode surface with a superimposed hexagonal array grid.

References

(1) Yang, F.; Nielander, A. C.; Grimm, R. L.; Lewis, N. S. Photoelectrochemical Behavior of N-Type GaAs(100) Electrodes Coated by a Single Layer of Graphene. *J. Phys. Chem. C* **2016**, *120* (13), 6989–6995. https://doi.org/10.1021/acs.jpcc.6b00232.

(2) Hu, S.; Shaner, M. R.; Beardslee, J. A.; Lichterman, M.; Brunschwig, B. S.; Lewis, N. S. Amorphous TiO_2 Coatings Stabilize Si, GaAs, and GaP Photoanodes for Efficient Water Oxidation. *Science* **2014**, *344* (6187), 1005–1009. https://doi.org/10.1126/science.1251428.

(3) Schneider, C. A.; Rasband, W. S.; Eliceiri, K. W. NIH Image to ImageJ: 25 Years of Image Analysis. *Nat. Methods* **2012**, *9* (7), 671–675. https://doi.org/10.1038/nmeth.2089.

(4) Zhao, Y.; Liu, W.; Bao, Y.; Ma, J.; Liu, Y.; Wang, X.; Yang, F. Direct Wafer Bonding of GaAs/Si by Hydrophobic Plasma-Activated Bonding. In *Eleventh International Conference on Information Optics and Photonics (CIOP 2019)*; Wang, H., Ed.; SPIE, 2019; p 232. https://doi.org/10.1117/12.2549964.

(5) Gabriel, M.; Johnson, B.; Suss, R.; Reiche, M.; Eichler, M. Wafer Direct Bonding with Ambient Pressure Plasma Activation. *Microsyst. Technol.* **2006**, *12* (5), 397–400. https://doi.org/10.1007/s00542-005-0044-4.

(6) Plach, T.; Hingerl, K.; Tollabimazraehno, S.; Hesser, G.; Dragoi, V.; Wimplinger, M. Mechanisms for Room Temperature Direct Wafer Bonding. *J. Appl. Phys.* **2013**, *113* (9), 094905. https://doi.org/10.1063/1.4794319.

(7) DeJarld, M.; Shin, J. C.; Chern, W.; Chanda, D.; Balasundaram, K.; Rogers, J. A.; Li, X. Formation of High Aspect Ratio GaAs Nanostructures with Metal-Assisted Chemical Etching. *Nano Lett.* **2011**, *11* (12), 5259–5263. https://doi.org/10.1021/nl202708d.

(8) Kennedy, K. M.; Kempler, P. A.; Cabán-Acevedo, M.; Papadantonakis, K. M.; Lewis, N. S. Primary Corrosion Processes for Polymer-Embedded Free-Standing or Substrate-Supported Silicon Microwire Arrays in Aqueous Alkaline Electrolytes. *Nano Lett.* **2021**, *21* (2), 1056–1061. https://doi.org/10.1021/acs.nanolett.0c04298.